The Astrophysical Journal, 793:91 (8pp), 2014 October 1 doi:10.1088/0004-637X/793/2/91

ON THE MASS OF THE LOCAL GROUP

Roberto E. González[1,2,3], Andrey V. Kravtsov[1,2,4], and Nickolay Y. Gnedin[1,2,5]
[1] Department of Astronomy & Astrophysics, The University of Chicago, Chicago, IL 60637, USA
[2] Kavli Institute for Cosmological Physics, The University of Chicago, Chicago, IL 60637, USA
[3] Instituto de Astrofísica, Pontificia Universidad Católica de Chile, Santiago, Chile; regonzar@astro.puc.cl
[4] Enrico Fermi Institute, The University of Chicago, Chicago, IL 60637, USA
[5] Particle Astrophysics Center, Fermi National Accelerator Laboratory, Batavia, IL 60510, USA
Received 2013 December 1; accepted 2014 July 28; published 2014 September 10

ABSTRACT

We use recent proper motion measurements of the tangential velocity of M31, along with its radial velocity and distance, to derive the likelihood of the sum of halo masses of the Milky Way and M31. This is done using a sample of halo pairs in the Bolshoi cosmological simulation of ΛCDM cosmology selected to match the properties and the environment of the Local Group. The resulting likelihood gives an estimate of the sum of the masses of $M_{\rm MW,200c} + M_{\rm M31,200c} = 2.40^{+1.95}_{-1.05} \times 10^{12}\,M_\odot$ (90% confidence interval). This estimate is consistent with individual mass estimates for the Milky Way and M31 and is consistent, albeit somewhat on the low side, with the mass estimated using the timing argument. We show that although the timing argument is unbiased on average for all pairs, for pairs constrained to have radial and tangential velocities similar to that of the Local Group the argument overestimates the sum of masses by a factor of 1.6. Using similar technique, we estimate the total dark matter mass enclosed within 1 Mpc from the Local Group barycenter to be $M_{\rm LG}(r < 1\,{\rm Mpc}) = 4.2^{+3.4}_{-2.0} \times 10^{12}\,M_\odot$ (90% confidence interval).

Key words: dark matter – Galaxy: fundamental parameters – Galaxy: halo – Local Group

Online-only material: color figures

1. INTRODUCTION

Understanding the connection between dark matter (DM) halos and the galaxies they host is a key question in galaxy formation theory. Theoretical models of hierarchical structure formation (White & Rees 1978; Fall & Efstathiou 1980; Blumenthal et al. 1984) envision DM halos to be the sites of galaxy formation and this framework is supported by a variety of observations (see, e.g., recent reviews by Frenk & White 2012; Courteau et al. 2014), such as galaxy rotation curves (Rubin & Ford 1970; Roberts & Rots 1973), X-ray halos (Forman et al. 1985; Buote & Canizares 1994; Buote et al. 2002; Humphrey et al. 2011; Bogdán et al. 2013, see Mathews & Brighenti 2003 for a review), satellite kinematics (Zaritsky et al. 1993, 1997; Zaritsky & White 1994; McKay et al. 2002; Prada et al. 2003; Conroy et al. 2007; Klypin & Prada 2009; More et al. 2011), and weak lensing measurements (e.g., Mandelbaum et al. 2006; van Uitert et al. 2011; Velander et al. 2013; Hudson et al. 2013).

The Local Group (LG hereafter) played an important role in establishing the existence of extended massive halos around galaxies. Indeed, the first flat rotation curve was measured for M31 (Babcock 1939) and the mass estimate for the LG by Kahn & Woltjer (1959) was one of the very first compelling indications for the existence of massive DM halos. The elegant argument in the latter study relied on the assumption that LG can be approximated by two point masses on a radial orbit on the first approach. Orbit integration backward in time, given the present day separation, velocity, and cosmological parameters, then constrains the mass of the system. This framework is now known as the timing argument (TA hereafter). Despite its simplicity and strong assumptions, the argument has withstood the test of time and new observations (Li & White 2008; van der Marel & Guhathakurta 2008; van der Marel et al. 2012). Nevertheless, the masses of both the Milky Way (MW) and M31 are both uncertain by a factor of two (e.g., Boylan-Kolchin et al. 2013 and references therein). Given the large uncertainties, the LG mass derived using the TA (Li & White 2008; van der Marel et al. 2012) is generally consistent with mass estimates derived using other methods (Klypin et al. 2002; Widrow & Dubinski 2005; Karachentsev et al. 2009; Watkins et al. 2010 and references therein), but is on the high side of the measurement range.

In this paper, we present a different way of constraining the mass of the LG using an approach similar to that used by Busha et al. (2011) to constrain the mass of the MW. In this approach, a set of observed properties of a system is used to estimate the likelihood that a system in the simulation is a counterpart of this system. The distribution of the likelihood as a function of halo mass can then be used to estimate the mass of the observed system. In this study, we select a population of the LG analogs from the Bolshoi cosmological simulation of ΛCDM cosmology (Klypin et al. 2011) and use the observed properties of the MW and M31 to derive the likelihood distribution for their combined mass.

We use several criteria to define the LG pair analogs in the cosmological simulation. In addition to distance and radial and tangential velocities, we also consider parameters characterizing environment, such as the distance to the nearest cluster, local large-scale density, and the coldness of the local galaxy flow. The LG is known to reside in a region of rather low ("cold") radial velocity dispersion of galaxies, $\sigma_{\rm H} < 70\,{\rm km\,s^{-1}}$ (Sandage & Tammann 1975; Governato et al. 1997; Karachentsev et al. 2003; Klypin et al. 2003; Aragon-Calvo et al. 2011 and references therein), as compared to velocity dispersion around MW-sized halos in the ΛCDM cosmology. This can be explained by the fact the LG is located in an average density environment (Klypin et al. 2003). We will explore in more detail this density and velocity dispersion relation, and use it to impose additional constrains to our LG analogs.

The paper is organized as follows. In Section 2, we describe the simulation and halo catalogs, while in Section 3

we describe the selection criteria for the LG analogs and different synthetic LG samples. We present our results for the likelihood distribution of the LG mass in Section 4 and compare mass estimated using this method with previous estimates using the TA in Section 5. We discuss our results and summarize our conclusions in Section 6. In this paper, we use mass, M_{200c}, defined as the mass within radius R_{200c} enclosing the mean density of 200 times the critical density at the redshift of analysis. For the MW-sized halos, M_{200c} is related to the commonly used virial mass definition defined using cosmology- and redshift-dependent overdensity Bryan & Norman (1998) as $M_{\rm vir}/M_{200c} \approx 1.2$.

2. SIMULATIONS AND HALO CATALOGS

To construct a sample of the LG analogs, we use halos from the Bolshoi simulation of ΛCDM cosmology: $\Omega_{\rm m} = 1 - \Omega_\Lambda = 0.27$, $H_0 = 70\,{\rm km\,s^{-1}\,Mpc^{-1}}$, $\sigma_8 = 0.82$, $n_s = 0.95$ (Klypin et al. 2011), compatible with the constraints from the *Wilkinson Microwave Anisotropy Probe* satellite (Hinshaw et al. 2013). The simulation followed the evolution of DM in a $250\,h^{-1}$Mpc box with a spatial resolution of $\approx 1\,h^{-1}$ kpc and a mass resolution of $m_{\rm p} = 1.35 \times 10^8\ M_\odot$. Halos are identified with the bound density maxima (BDM) algorithm (Klypin & Holtzman 1997). The BDM algorithm is a spherical overdensity halo-finding algorithm and is designed to identify both host halos and subhalos. In this study, however, we will only use the host halos.

The catalog of host halos is complete down to halos with maximum circular velocities of $\approx 50\ {\rm km\,s^{-1}}$, and we use only halos of larger mass to identify pairs of the MW-sized halos. To construct a sample of the MW–M31 pairs at $z \approx 0$, we use a series of simulation snapshots at $z < 0.1$ (i.e., in the last $\approx$1.3 Gyr before the present) spaced by $\approx$150–250 Myr, similar to the strategy adopted in González et al. (2013). This is done because a particular configuration of MW and M31 is transient and would correspond to a relatively small number of systems at one snapshot. By using multiple snapshots, we can increase the sample of systems in such configuration during a period of time in which secular cosmological evolution is small. For instance, the average mass growth of MW-sized halos in the simulation since $z = 0.1$ is only 1.2%.

3. THE SAMPLE OF LOCAL GROUP ANALOGS

The LG is dominated by the pair of the MW and M31 galaxies and includes a number of smaller galaxies. The environment around the LG has a density quite close to the average density of the universe (Klypin et al. 2003; Karachentsev 2005, 2012). In addition, the closest massive galaxy cluster, the Virgo Cluster, is $\approx$16.5 Mpc away (Mei et al. 2007). It is not clear to what extent the environment of the LG shapes its properties and dynamics. Therefore, we include its environmental criteria in our set of selection criteria.

In order to identify the LG analogs, we select pairs in relative isolation and in a wide range of masses from $M_{200c} = 5 \times 10^{10}\ M_\odot$ to $5 \times 10^{13}\ M_\odot$. To avoid pairs in triplets or larger groups, we define a quantitative isolation criterion using the force constraint $F_{i,{\rm com}} < \kappa\, F_{12}$, where $F_{i,{\rm com}}$ is the gravitational force between the pair and any neighbor halo i within a $5\,h^{-1}$Mpc radius of the pair center of mass, F_{12} is the force between the pair, and κ is a constant parameter. The isolation criterion becomes increasingly strict for decreasing values of κ. The MW and M31 do not have massive neighbors within 5 Mpc, and should thus have $\kappa < 0.1$. The actual value of κ is, however, uncertain, and we use $\kappa = 0.25$ based on our previous tests reported in González et al. (2013).

An additional selection criterion is intended to mimic the absence of massive clusters in the immediate vicinity of the LG. We require that halos in the LG sample have no neighbor halo with a mass $M_{200c} > 1.5 \times 10^{14}\ M_\odot$ within 12 Mpc. The mass and distance limits are somewhat lower than the actual values for the Virgo Cluster (e.g., Fouqué et al. 2001; Nulsen & Bohringer 1995 and references therein) to allow for a larger number of systems.

We found 4177 pairs in the snapshot at $z = 0$ under these constraints, and for the full composite sample using 10 more snapshots at $z < 0.1$, we found 45,844 pairs,[6] which we use as the sample of LG analogs. We find that ≈80% of LG analogs in this sample are gravitationally bound under the two-body approximation. Note that the environment criteria are very restrictive: from the initial sample of pairs selected only by mass and separation, less than 1% satisfy the environment criteria.

4. MASS LIKELIHOOD

To compute the likelihood distribution for the MW–M31 pairs using the sample of the LG analogs, we follow the approach of Busha et al. (2011), but with modifications described in González et al. (2013). Namely, to compute the likelihood, we first select a sample of LG-like pairs satisfying a particular combination of constraints. For each combination of constraints, the mass likelihood, $P(M)$, is then computed as the normalized distribution of the pair mass. Note that this is different from the procedure used by Busha et al. (2011), because we compute the likelihood for several combined constraints as the direct mass distribution of halo pairs, rather than multiplying the likelihood distributions for individual constraints as was done by Busha et al. (2011). Thus, in our procedure, we do not assume that the properties used in different constraints are uncorrelated. Any correlation between constraints is included in the total likelihood.

The specific properties we use in our constraints to define LG pair samples and to construct the mass likelihood for different combinations of constraints are as follows.

1. Galactocentric radial velocity, $V_{\rm RAD} = 109.3 \pm 4.4\ {\rm km\,s^{-1}}$, of M31 measured recently by Sohn et al. (2012). We include in the pairs radial peculiar velocities, the Hubble flow at a companion distance so we do take into account the Hubble expansion correction.
2. Distance between M31 and MW, $\Delta r = 770 \pm 40$ kpc, adopted by van der Marel & Guhathakurta (2008) to span the range of recent measurements using different methods, the tip of the red giant branch (Durrell et al. 2001; McConnachie et al. 2005), cepheids (Joshi et al. 2003; Karachentsev et al. 2004), and eclipsing binaries (Ribas et al. 2005).
3. The tangential velocity component of M31 relative to the MW is $V_{\rm TAN} = 17\ {\rm km\,s^{-1}}$, where the 1σ upper limit is $V_{\rm TAN} < 34.3\ {\rm km\,s^{-1}}$ recently derived by Sohn et al. (2012).
4. We use the local environmental constraint using the local velocity dispersion, $\sigma_{\rm H}$, and logarithm of the overdensity $\log(1+\delta)$ in a shell with an inner radius of 1 Mpc, and an outer radius of 5 Mpc from the pair center of mass. We

[6] Some of these pairs are not independent are repeated in other snapshots, but after including the additional constraints, it is extremely unlikely that any are repeated. Nevertheless, if any repeats are identified, they are removed at this stage.

Table 1
Mass Likelihood of MW + M31 Pairs in LG Analogs

Constraints	$\log(M_{200c}/M_\odot)$	68% Conf. Interval	90% Conf. Interval	N Pairs
$V_{\rm RAD} + \Delta r$	12.60	−0.10 +0.12	−0.31 +0.45	347
$V_{\rm RAD} + \Delta r + V_{\rm TAN}$	12.45	−0.12 +0.11	−0.25 +0.25	88
$V_{\rm RAD} + \Delta r + V_{\rm TAN} + \log(1+\delta)$	12.38	−0.07 +0.09	−0.25 +0.24	66
$V_{\rm RAD} + \Delta r + V_{\rm TAN} + \sigma_{\rm H}$	12.39	−0.07 +0.13	−0.19 +0.27	64
$V_{\rm RAD} + \Delta r + V_{\rm TAN} + \log(1+\delta) + 1$ Mpc	12.62	−0.11 +0.13	−0.28 +0.26	66
$V_{\rm RAD} + \Delta r + V_{\rm TAN} + \sigma_{\rm H} + 1$ Mpc	12.62	−0.11 -0.13	−0.28 +0.27	64

use the constraint of $\sigma_{\rm H} < 70\,{\rm km\,s^{-1}}$ to reflect the range of observational estimates (see Section 1). In Appendix A, we show that the velocity dispersion is correlated with overdensity, and that our fiducial choice of $\sigma_{\rm H} < 70\,{\rm km\,s^{-1}}$ approximately corresponds to the upper limit on overdensity $\log(1+\delta) < 0.3$.

Our fiducial choice for the mass constraints presented in the paper is to use the range of observed values of constraint parameters with intervals corresponding to $\pm 2\sigma$ of their observational errors. Namely, we use the following rms uncertainties: $\sigma_{V_{\rm RAD}} = 4.4\,{\rm km\,s^{-1}}$ for radial velocity and $\sigma_{\Delta r} = 40$ kpc for separation. We do not have complete information about the confidence interval for the tangential velocity and we use the estimate of the average tangential velocity of $17\,{\rm km\,s^{-1}}$ and its 1σ upper limit of $V_{\rm TAN} < 34.3\,{\rm km\,s^{-1}}$ to extrapolate to 2σ the upper limit of $V_{\rm TAN} < 51.6\,{\rm km\,s^{-1}}$, and 3σ of $V_{\rm TAN} < 68.6\,{\rm km\,s^{-1}}$.

With these assumptions, we select the pairs with corresponding properties p lying in the interval $p \pm 2\sigma_p$. Thus, for example, for the first constraint in Table 1, which uses the combination of radial velocity and pair separation, we select all halo pairs that satisfy isolation criteria described in the previous section and have relative radial velocity $V_{\rm RAD} = 109.3 \pm 8.8\,{\rm km\,s^{-1}}$ and $\Delta r = 770 \pm 80$ kpc. The mass likelihood distribution for the pair sample selected using properties within these intervals is then simply the normalized mass distribution of pairs in the sample.

We have explored the effect of expanding our sample of pairs by increasing the interval in radial velocity, separation, and tangential velocity we use to select pairs to $p \pm 3\sigma_p$ and found that the mass likelihood is stable. A more detailed description of the tests for different constraints ranges can be found in the Appendix B.

Figure 1 shows the likelihood distribution for the sum of M_{200c} masses of the two pair halos obtained for different constraint combinations. In Table 1, we present the corresponding median values, with 68% and 90% confidence intervals and the number of pairs in each sample. In addition, we present the constraints on the mass within the radius of 1 Mpc from the pair barycenter in the last two rows of the table.

Figure 1 shows that the radial velocity of M31 provides the main constraint on the masses. Nevertheless, the inclusion of the tangential velocity constraint eliminates the tail of objects at very high masses and shifts the peak of the likelihood to lower masses. This is because imposing the constraint of a low tangential velocity removes more massive pairs with higher orbital energies for a given fixed range of radial velocities.

The local density and velocity dispersion constraints do not affect the peak of the likelihood distribution, but slightly narrow the width of the likelihood. Overall, we find that the inclusion of the environmental constraints in the likelihood calculations makes no significant difference: they shift the median and confidence intervals to masses ≈15% lower.

We have explored the mass ratio distribution[7] for different samples following constraints from Table 1 and found no effect of additional constraints on the mass ratio on the mass likelihood.

We also compute the statistical errors in the shape of the distribution due the low number of pairs in the samples. In Figure 2, we show errors for the two most relevant samples: $V_{\rm RAD} + \Delta r + V_{\rm TAN}$ (red) and $V_{\rm RAD} + \Delta r + V_{\rm TAN} + \log(1+\delta)$ (black). We see that there is no significant effect on the width of both distributions produced by the statistical errors; however, the bimodality shape observed for the red curve is more likely to be a fluctuation due to errors rather than a real feature.

5. COMPARISON WITH THE PREVIOUS TIMING ARGUMENT MASS ESTIMATES

Li & White (2008, hereafter LW08) computed the bias and error distribution of the TA estimator using LG-like systems in the Millennium Simulation. On average, they found good matches between the true M_{200c} masses of the MW + M31 halos and the $M_{\rm TA}$ masses: $M_{\rm TA} = 5.32 \pm 0.48 \times 10^{12}\,M_\odot$, or $\log M_{\rm TA}/M_\odot = [12.68, 12.76]$, which does not even overlap with our best 90% confidence interval from Table 1 (third row). However, if we compute the TA mass using Equations (1)–(3) from their paper, but with updated radial velocity and separation values, we obtain a somewhat lower value of $M_{\rm TA} = 4.14 \pm 0.60 \times 10^{12}\,M_\odot$ ($\log M_{\rm TA}/M_\odot = [12.55, 12.68]$), in good agreement with van der Marel et al. (2012). The decrease is primarily due to the lower radial velocity value compared to that used by LW08. Therefore, the TA mass range computed with updated velocity values is in good agreement with our likelihood estimate without taking into account the tangential velocity and local environment (first line in Table 1). The somewhat lower estimate in our analysis is then primarily due to the tangential velocity and environmental constraints, which shift the peak of the likelihood to smaller masses.

In Figure 3, we show distribution of the ratio, $A_{200} = M_{200c}({\rm MW+M31})/M_{\rm TA}$ (after LW08), of the true pair mass and the TA mass for different samples of LG analogs.[8] The LG analog sample with an additional cut of $150 < V_{\rm max} < 300\,{\rm km\,s^{-1}}$ (corresponding to the broad $V_{\rm max}$ selection of LW08) shows a distribution with a median $A_{200} \approx 1.1$. If we use a narrower $V_{\rm max}$ range, the distribution also becomes

[7] Defined as the ratio between the halo mass of the smallest and largest pair member. The mass ratio of the MW/M31 pair is quite uncertain, but recent papers point toward a mass ratio close to unity, where M31 is somewhat more massive than the MW (Karachentsev et al. 2009; Reid et al. 2009; Baiesi Pillastrini 2009).

[8] The TA estimate is computed using the age of the universe at $z = 0$ even if some pairs are found at $z > 0$, but using the corrected age for them makes very little difference and surely the MW and M31 did not start evolving at $a = 0$, so using the current age of the universe is an overestimate anyway.

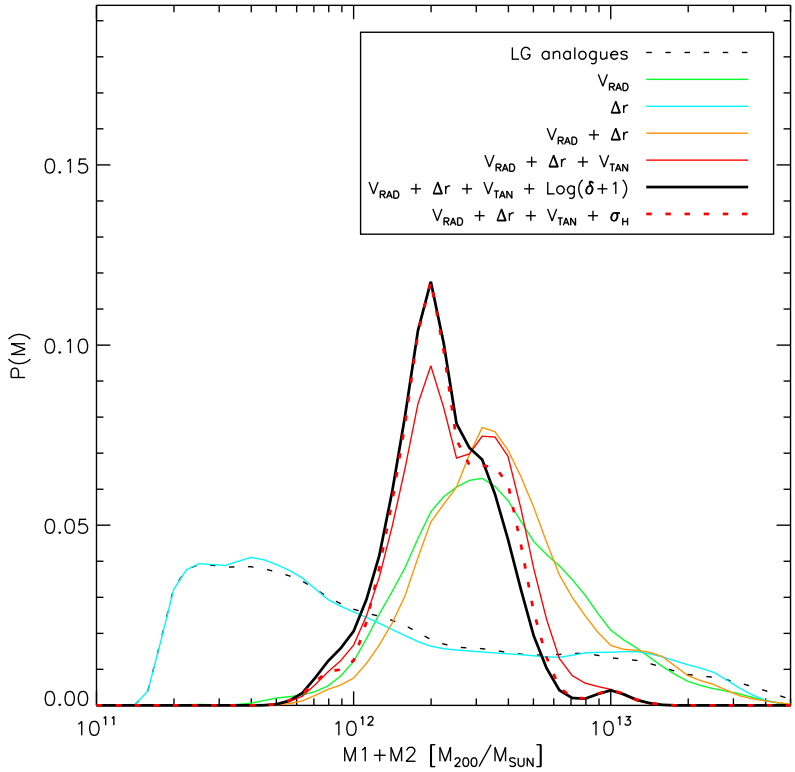

Figure 1. Likelihood distribution for the sum of M_{200c} masses (mass within radius enclosing density equal to $200c$ times the critical density of the universe) of MW and M31 constructed using the LG halo pair analogs and using observational measurements of the relative separation and motion of MW and M31 with intervals corresponding to 2σ of their measurement errors, as well as constraints on their environment (see the legend). The median mass and corresponding 68% and 90% confidence intervals for each set of constraints are given in Table 1.

(A color version of this figure is available in the online journal.)

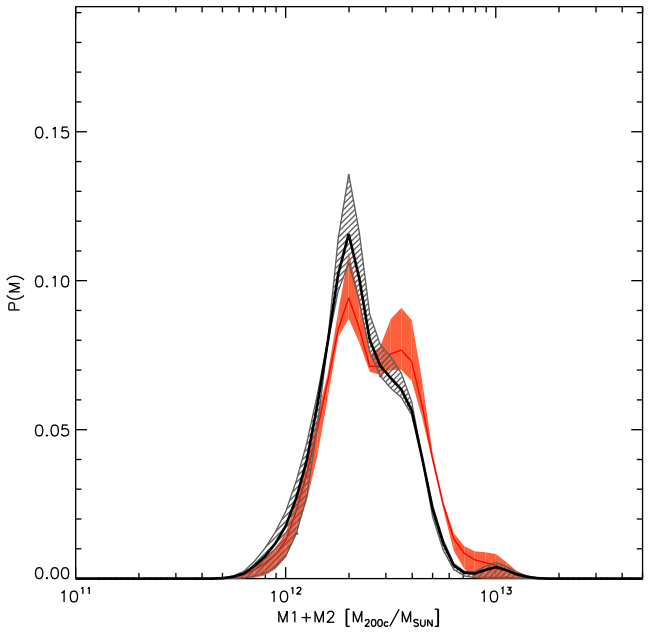

Figure 2. Likelihood distribution for the sum of M_{200} masses, similar to Figure 1 for the $V_{\rm RAD}+\Delta r+V_{\rm TAN}$ (red) and $V_{\rm RAD}+\Delta r+V_{\rm TAN}+\log(1+\delta)$ (black) samples. The error contours computed using a jackknife estimator are included. There is no significant effect on the width of both distributions produced by the statistical errors of the sample size.

(A color version of this figure is available in the online journal.)

narrower, in agreement with the results of LW08 (see their Figures 1 and 2). For the radial velocity and distance constraint (orange), the median $A_{200} \approx 0.97$, but with a similar scatter.

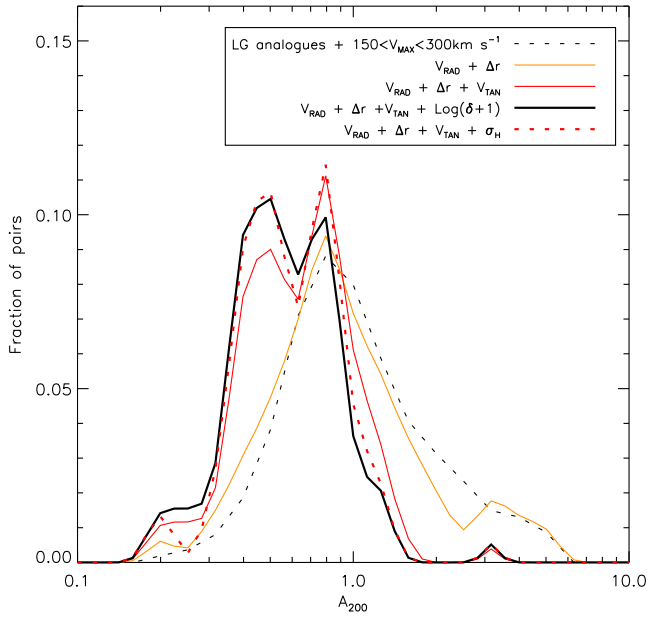

Figure 3. Ratio of the true pair mass and the TA mass estimate, A_{200}, for different combinations of constraints. In the case of radial velocity and separation constraints (orange), the median A_{200} is close to unity, but when the tangential velocity constraint is included, the TA overestimates the true mass, pushing the distribution to lower A_{200} values.

(A color version of this figure is available in the online journal.)

Including the tangential velocity constraint in the selection of pairs (solid red) results in a narrow distribution of the median shifted to a smaller value of $A_{200} \approx 0.75$, while the inclusion of the additional local density or velocity dispersion

constraint shifts the median to $A_{200} \approx 0.62$. This explicitly shows that the TA estimates work quite well for average halo pairs of separations and radial velocity. However, pairs with additional constraints on the tangential velocity and local density have systematically lower masses compared to the TA estimate. In other words, for such pairs, the TA estimate overestimates the mass by a factor of ≈1.3–1.6. This explains the systematic difference between our fiducial constraint from the likelihood, $\log M_{200c}(\mathrm{MW+M31}) \approx 12.38^{+0.09}_{-0.07}$ and the TA estimate $\log M_{200c}(\mathrm{MW+M31}) \approx 12.62^{+0.06}_{-0.07}$.

There are discrepancies between our results and those of LW08. In particular, LW08 show in their Figure 6 that the median A_{200} does not decrease significantly for $V_{\rm TAN} < 86\,\mathrm{km\,s^{-1}}$. However, we find that A_{200} depends on the mass distribution of halos in the sample, decreasing with decreasing halo mass. In addition, we find that the sensitivity of the A_{200} on $V_{\rm TAN}$ constraint also depends on the median mass and the mass range of the sample: for halo samples with narrower mass ranges, the effect of the $V_{\rm TAN}$ on A_{200} is weaker.

Specifically, for different mass ranges (masses in units of $M_{200c}/10^{12}\,M_\odot$), we measure the median value, $\overline{A}_{200}$: $M = [0.5, 1.0]$ then $\overline{A}_{200} = 0.62$; $M = [1.0, 1.5]$ then $\overline{A}_{200} = 0.71$; $M = [1.75, 2.25]$ then $\overline{A}_{200} = 0.90$; $M = [2.0, 3.0]$ then $\overline{A}_{200} = 1.06$; $M = [3.0, 5.0]$ then $\overline{A}_{200} = 1.22$. Thus, we find that A_{200} depends on the halo mass of the halos in the pair. Therefore, because the inclusion of $V_{\rm TAN}$ constraint lowers the masses of the halos in the sample, we obtain a lower value of $\overline{A}_{200}$. We also made tests for wider ranges of $V_{\rm RAD}$ or Δr and find that the wider range does not significantly change the average mass of the underlying mass distribution and median A_{200} values.

Our LG analogs are allowed in a wide range of masses (see Section 3), and our main sample (Row 3, Table 1) contains pairs with masses within the range $[1.4, 4.4] \times 10^{12}\,M_\odot$, with an average mass of $\approx 2.4 \times 10^{12}\,M_\odot$. Given that we do not constrain individual masses of each pair member, the individual halo masses can span a wide mass range from ∼0.1 to $4.4 \times 10^{12}\,M_\odot$ with an average mass of $\sim 1.2 \times 10^{12}\,M_\odot$. Thus, they include rather small halos. In contrast, LW08 halo masses lie in the range $[0.8, 7] \times 10^{12}\,M_\odot$ for each pair member, with an average halo mass of $\sim 2.5 \times 10^{12}\,M_\odot$.[9] So the LW08 sample has a narrower mass range and a higher average mass, which is the reason they find a weak sensitivity of A_{200} to the $V_{\rm TAN}$ constraint. For the mass range and average mass of the LW08 sample, our test results for the halo sample with an average mass of $\sim 2.5 \times 10^{12}\,M_\odot$ gives a value of $\overline{A}_{200} = 1.06$, which is quite consistent with LW08.

It is worth noting that it is quite surprising that the TA estimate works to within a factor of two, given how idealized the model underlying such estimate is. For example, MW and M31 are approximated as point masses of constant mass on a purely radial orbit and the surrounding mass distribution is neglected. At the same time, the mass evolution of MW and M31 is neglected as well. Finally, the evolution of MW and M31 is envisioned within the expanding background corresponding to the mean density of the universe and thus any dependence of expansion on the local overdensity is neglected. Given the simplicity of the model and a number of assumptions, it is quite remarkable that this model provides a reasonable ballpark estimate of mass. However, sensitivity to the tangential velocity and the environment that we find shows that the accuracy of the TA estimate is ultimately limited.

Finally, we note that the mass estimate we derive from the likelihood is in reasonably good agreement with the recent abundance matching results (Kravtsov et al. 2014, see their Appendix), which for the stellar masses of $5 \times 10^{10}\,M_\odot$ and $9 \times 10^{10}\,M_\odot$ for MW and M31, respectively, indicate an average halo mass of $M_{200}(\mathrm{MW+M31}) \approx 4.3 \times 10^{12} M_\odot$ (or $\log_{10} M_{200c}(\mathrm{MW+M31}) \approx 12.6$). This abundance matching result is based on the new measurement of the stellar mass function by Bernardi et al. (2013), which corrects significant photometric errors in the standard Sloan Digital Sky Survey (SDSS) magnitudes. The average scatter around this average value is thought to be ≈0.2 dex, and although the scatter is large, the agreement is encouraging, especially because previous abundance matching results by Moster et al. (2013) and Behroozi et al. (2013), based on older estimates of the stellar mass functions with SDSS photometry, indicated a very large average mass of $M_{200c}(\mathrm{MW+M31}) \approx 8$–$10 \times 10^{12} M_\odot$ for the stellar masses of MW and M31. Reconciling the low mass of the LG with abundance matching results would require the assumption that MW and/or M31 are outliers from the average M_*–M_{200c} relation. However, better agreement with the new abundance matching M_*–M_{200c} based on the stellar mass function of Bernardi et al. (2013) indicates that the halo masses of MW and M31 are consistent with the masses expected from the mean M_*–M_{200c} relation.

6. DISCUSSION AND CONCLUSIONS

We define the LG analogs in the Bolshoi simulation of ΛCDM cosmology and estimate the MW–M31 pair mass likelihood in such systems. The analogs are selected as halo pairs using broad criteria. The sample is then used to estimate likelihood distribution of mass using several observed properties of the actual LG, namely, separation, radial and tangential velocity, and density of the local environment. To characterize the latter, we compute the DM overdensity and particle velocity dispersion, $\sigma_{\rm H}$, within 5 Mpc from halo pair center of mass. We found a tight correlation between local overdensity and velocity dispersion estimated within 5 Mpc (see Appendix A), so that the constraint on overdensity is approximately equivalent to the constraint on the velocity dispersion. To set the environmental constraint, we require $\sigma_{\rm H} < 70\,\mathrm{km\,s^{-1}}$ (or $\log(\delta+1) < 0.3$) based on the observational values of this dispersion reported in the literature. At a given snapshot around $z = 0$, about 2% of the MW-sized ($M_{200} \sim 10^{12}\,M_\odot$) halos satisfy our broad LG analog criteria, and less than 5% of these 2% satisfy the additional orbital and environmental constraints.

We have shown that the main parameter controlling the MW–M31 mass likelihood is radial velocity. However, we also show that the likelihood is sensitive to the constraints on tangential velocity. In particular, we find that mass likelihood peak shifts to lower masses when the constraint on the tangential velocity is included. This is because this constraint eliminates massive pairs with a given radial velocity range. Note that there is no such sensitivity to the tangential velocity in the TA estimate because neither the tangential velocity nor the environment are taken into account in such an estimate. Indeed, the mass constrain we derive from the likelihood is in good agreement with the mass estimate from the TA when only radial velocity and separation are used as constraints: $M_{\rm TA} = 4.14 \pm 0.60 \times 10^{12}\,M_\odot$, in agreement with van der Marel et al. (2012) results, but somewhat lower than LW08 due to the lower updated value

[9] We convert LW08 $V_{\rm MAX}$ ranges to M_{200c} by computing the relation directly from the simulation.

of the radial velocity used in our estimate. However, when we add the tangential velocity and environmental constraints, the median of the likelihood shifts to lower masses by a factor of ≈1.6. We explicitly show that for pairs with low tangential velocities and low local overdensity and velocity dispersion, the TA overestimates the true masses of the pair by an average factor of ≈1.6, thereby explaining the lower values derived from the likelihood method. These values are summarized in Table 1: our fiducial mass estimate obtained, including the local density constraint, is $M_{\rm MW,200c}+M_{\rm M31,200c}=2.40^{+0.55}_{-0.36}\times10^{12}M_\odot$ (68% confidence interval). For this sample, we have also computed the DM mass enclosed within 1 Mpc from the pair center of mass: $M_{\rm LG}(r<1\,{\rm Mpc})=4.17^{+1.45}_{-0.93}\times10^{12}M_\odot$ (68% confidence interval).

Overall, the values we deduce for the sum of the MW and M31 halo masses are consistent with the existing constraints on the individual halo masses of the MW (see, e.g., Boylan-Kolchin et al. 2012, 2013 and references therein) and M31 (Widrow & Dubinski 2005). Given that the estimates of halo mass using satellite velocity (e.g., Boylan-Kolchin et al. 2013) can give robust lower limits to individual halo masses, the combination of the estimates of the combined LG mass and individual masses should help to narrow down the range of possible masses for our Galaxy and for our closest neighbor, M31.

We thank Anatoly Klypin for making the Bolshoi simulation and the BDM halo catalogs publicly available. This work was supported by the NSF via grant OCI-0904482. A.K. was also supported in part by the NSF grant AST-0807444 and by the Kavli Institute for Cosmological Physics at the University of Chicago through the NSF grants PHY-0551142 and PHY-1125897 and an endowment from the Kavli Foundation. We have made extensive use of the NASA Astrophysics Data System and `arXiv.org` preprint server.

APPENDIX A

COLD LOCAL HUBBLE FLOW

In order to characterize the local environment of the LG, we use the velocity dispersion $\sigma_{\rm H}$ of nearby galaxies. It is known that this velocity dispersion is rather low within a few megaparsecs from the LG, compared to the velocity dispersion expected for MW-sized halos in simulations (e.g., Governato et al. 1997). This "coldness" of the local Hubble flow was noted for quite some time in studies measuring the Hubble constant with local galaxies (de Vaucouleurs 1958; Sandage & Tammann 1975). The values of velocity dispersion were consistently found to be around $\sigma_{\rm H}\sim60\,{\rm km\,s^{-1}}$ up to 8 Mpc (Sandage & Tammann 1975; Giraud 1986; Ekholm et al. 2001; Karachentsev et al. 2009, 2003; Macciò et al. 2005; Tikhonov & Klypin 2009; Klypin et al. 2003; Aragon-Calvo et al. 2011). However, the local velocity dispersion increases with the maximum radius adopted to measure it (Sandage & Tammann 1975; Macciò et al. 2005; Tikhonov & Klypin 2009), and thus the specific value of the velocity dispersion used for constraints should correspond to the radius used in observations.

Furthermore, the methodology to compute the local velocity dispersion must also be taken into account when comparing different results; i.e., Karachentsev et al. (2003) found $\sigma_{\rm H}=85\,{\rm km\,s^{-1}}$ within 5 Mpc, but the estimate drops to $\sigma_{\rm H}=41\,{\rm km\,s^{-1}}$ when members of the M81 and Cen A groups are removed. We adopt the conservative value of $\sigma_{\rm H}<70\,{\rm km\,s^{-1}}$ as a constraint for the mass likelihood computation. The coldness of the local flow can be attributed to the relative isolation of the LG, and the relatively low density of the LG environment (Klypin et al. 2003; Martinez-Vaquero et al. 2009).

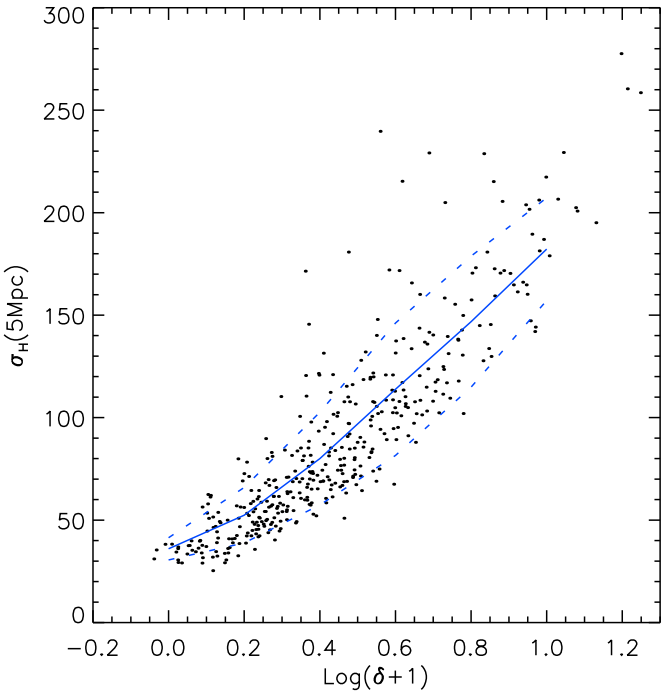

Figure 4. Local overdensity and velocity dispersion relation for the MW-sized halos in the LG analogs sample. The blue lines show the mean and the standard deviation of the distribution. Density and velocity dispersion are computed using DM particles within a shell ranging from 1 to 5 Mpc.

(A color version of this figure is available in the online journal.)

Macciò et al. (2005) found a correlation between $\sigma_{\rm H}$ and the local density in ΛCDM numerical simulations and pointed out that observational velocity dispersion measurements around the LG imply an overdensity of $-0.1<\delta\rho/\rho<0.6$ on the scale of 7 Mpc. We explore the $\sigma_{\rm H}$–overdensity relation for our sample of LG analogs, estimating $\sigma_{\rm H}$ using halos and DM particles with respect to the pair center of mass. For the former, we compute the radial peculiar velocity of host halos with maximum circular velocities of $V_{\rm max}>50\,{\rm km\,s^{-1}}$. For the latter estimate, we use DM particles outside $3\times R_{200}$ from any halos with $V_{\rm max}>50$.

Halos should be closer to galaxy tracers used in observations, but for some pairs the number of halos is too low for an adequate $\sigma_{\rm H}$ computation. On the other hand, using particles gives a robust $\sigma_{\rm H}$ computation in all cases, but makes comparison with observations more ambiguous. There is an overall scatter of $\sim40\,{\rm km\,s^{-1}}$ between the two estimates of $\sigma_{\rm H}$, which decreases to $\approx25\,{\rm km\,s^{-1}}$, for velocity dispersions lower than $100\,{\rm km\,s^{-1}}$. In both cases, $\sigma_{\rm H}$ is computed in shells with radii ranging within 1–5 Mpc. The lower limit is set because the Hubble flow is observed only at $R_0\gtrsim1$ Mpc (e.g., Karachentsev 2012). This can be used to put an upper limit to the mass of the LG (Ekholm et al. 2001; Karachentsev et al. 2002, 2009).

In Figure 4, we show the $\sigma_{\rm H}$–overdensity relation estimated around the LG analogs, in which each pair member is in the mass range of $0.8–2.9\times10^{12}\,M_\odot$ chosen to follow sample definition from González et al. (2013). We see a fairly tight relation at low $\sigma_{\rm H}$ values, in agreement with Macciò et al. (2005) with 20%, 43%, and 65% of the LG analogs having $\sigma_{\rm H}$ lower than 50, 70, and $100\,{\rm km\,s^{-1}}$, which corresponds to the average overdensities of $\log(1+\delta)=0.156$, 0.237, and 0.303, respectively. For the

mass likelihood estimate, we use the constraint $\log(1+\delta) < 0.3$ corresponding to systems with $\sigma_H < 70\,\mathrm{km\,s^{-1}}$ on average.

APPENDIX B

SENSITIVITY OF THE MASS LIKELIHOOD DISTRIBUTION TO CONSTRAINT CHOICES

The pair separation, radial, and tangential velocity are the main orbital constraints used for the mass likelihood computation. They are very restrictive due their small associated errors resulting in a small number of halo pairs. The samples can be increased if we relax these constraints and instead assume that the errors for a particular parameter are two or three times larger than the actual errors. In this section, we investigate the effect of such choices used as a constraint in the calculation of the likelihood distribution. A larger adopted error allows us to increase the size of the halo samples and decrease the associated Poisson errors. However, it means that we allow for the inclusion of objects less consistent with observational constraints. The actual choice of the error is a trade off between these two considerations.

The 1σ error for distance and radial velocity are $\sigma(\Delta r) = 40$ kpc and $\sigma(V_{\rm RAD}) = 4.4\,\mathrm{km\,s^{-1}}$. The mean value of the tangential velocity is $17\,\mathrm{km\,s^{-1}}$ with a 1σ upper limit of $V_{\rm TAN} < 34.3\,\mathrm{km\,s^{-1}}$, which we extrapolate to 2σ and 3σ upper limits of $V_{\rm TAN} < 51.6\,\mathrm{km\,s^{-1}}$ and $V_{\rm TAN} < 68.6\,\mathrm{km\,s^{-1}}$, respectively. We repeat our likelihood calculations using the errors of the constraint parameter separately inflated by a factor of three for each constraint and for all combined constraints. Here we do not include environmental constraint, given that we found that their effect is relatively small.

In the first test, we keep the errors for distance and tangential velocity fixed to their respective 1σ values, while we change the error of $\sigma(V_{\rm RAD})$. The results are listed in Table 2, which shows that the median mass value increases when the error of the radial velocity is increased from $\pm 4.4\,\mathrm{km\,s^{-1}}$ to $8.8\,\mathrm{km\,s^{-1}}$, but is not sensitive to further increase due to the combined constraints of all of the other parameters. The 68% and 90% confidence intervals also increase somewhat with increasing error. The number of pairs increase from 12 to 60 for 1σ to 4σ values.

In the second test, we have kept the errors of radial and tangential velocity fixed at 1σ, but increased the error of distance, $\sigma(\Delta r)$ (Table 3). The median mass and 68% confidence interval are not sensitive to increases in the distance errors, while the 90% confidence interval increases somewhat. At 3σ the number of pairs increases to 40.

In the third test, we have kept the radial velocity and separation errors fixed at 1σ, while varying the adopted error of $\sigma(V_{\rm TAN})$ (Table 4). The increase of the tangential velocity constraint to $51.6\,\mathrm{km\,s^{-1}}$ (2σ) does not change the median, while the increase to $68.6\,\mathrm{km\,s^{-1}}$ (3σ) leads to an increase of the median mass value and the confidence intervals. The number of pairs increases to 20 and 31 for 2σ and 3σ, respectively.

Finally, when we vary errors of all of the constraining parameters simultaneously (Table 5), the median mass value increases by less than 1σ when errors are inflated by a factor of two. The main effect on the confidence intervals is to increase the range of mass values smaller than the median, while the upper error bar does not change and even decreases slightly.

Table 2
Mass Likelihood Dependence on $V_{\rm RAD}$ Constraint Amplitude

$\sigma(V_{\rm RAD})/(4.4\,\mathrm{km\,s^{-1}})$	$\log(M_{200}/M_\odot)$	90% Conf. Interval	68% Conf. Interval
1.0	12.38	−0.13 +0.29	−0.05 +0.19
1.5	12.35	−0.29 +0.32	−0.10 +0.17
2.0	12.51	−0.31 +0.27	−0.19 +0.11
2.5	12.48	−0.28 +0.22	−0.17 +0.12
3.0	12.51	−0.31 +0.19	−0.17 +0.09
3.5	12.51	−0.32 +0.27	−0.17 +0.09
4.0	12.51	−0.40 +0.28	−0.17 +0.11

Table 3
Mass Likelihood Dependence on Δr Constraint Amplitude

$\sigma(\Delta r)/(40$ kpc)	$\log(M_{200}/M_\odot)$	90% Conf. Interval	68% Conf. Interval
2.0	12.36	−0.12 +0.31	−0.04 +0.17
3.0	12.37	−0.24 +0.30	−0.07 +0.13

Table 4
Mass Likelihood Dependence on $V_{\rm TAN}$ Constraint Amplitude

$V_{\rm TAN}/(\mathrm{km\,s^{-1}})$	$\log(M_{200}/M_\odot)$	90% Conf. Interval	68% Conf. Interval
51.6	12.38	−0.14 +0.39	−0.07 +0.20
68.6	12.54	−0.29 +0.23	−0.19 +0.05

Table 5
Mass Likelihood Dependence on Increasing All Constraints Amplitudes

$\sigma(\mathrm{test})/\sigma$	$\log(M_{200}/M_\odot)$	90% Conf. Interval	68% Conf. Interval
1.0	12.38	−0.13 +0.29	−0.05 +0.19
2.0	12.45	−0.25 +0.25	−0.12 +0.11
3.0	12.44	−0.32 +0.27	−0.13 +0.11

These tests indicate that our results for the mass likelihood do not depend sensitively to our fiducial choice to inflate the observed errors by a factor of two. In fact, if anything, the derived mass constraint for the actual observational errors is slightly smaller with smaller error bars. In this case, however, the sample contains only 12 pairs. We therefore believe that our fiducial choice is more conservative.

REFERENCES

Aragon-Calvo, M. A., Silk, J., & Szalay, A. S. 2011, MNRAS, 415, L16
Babcock, H. W. 1939, LicOB, 19, 41
Baiesi Pillastrini, G. C. 2009, MNRAS, 397, 1990
Behroozi, P. S., Wechsler, R. H., & Conroy, C. 2013, ApJ, 770, 57
Bernardi, M., Meert, A., Sheth, R. K., et al. 2013, MNRAS, 436, 697
Blumenthal, G. R., Faber, S. M., Primack, J. R., & Rees, M. J. 1984, Natur, 311, 517
Bogdán, Á., Forman, W. R., Vogelsberger, M., et al. 2013, ApJ, 772, 97
Boylan-Kolchin, M., Bullock, J. S., & Kaplinghat, M. 2012, MNRAS, 422, 1203
Boylan-Kolchin, M., Bullock, J. S., Sohn, S. T., Besla, G., & van der Marel, R. P. 2013, ApJ, 768, 140
Bryan, G. L., & Norman, M. L. 1998, ApJ, 495, 80
Buote, D. A., & Canizares, C. R. 1994, ApJ, 427, 86
Buote, D. A., Jeltema, T. E., Canizares, C. R., & Garmire, G. P. 2002, ApJ, 577, 183
Busha, M. T., Marshall, P. J., Wechsler, R. H., Klypin, A., & Primack, J. 2011, ApJ, 743, 40
Conroy, C., Prada, F., Newman, J. A., et al. 2007, ApJ, 654, 153
Courteau, S., Cappellari, M., de Jong, R. S., et al. 2014, RvMP, 86, 47
de Vaucouleurs, G. 1958, AJ, 63, 253
Durrell, P. R., Harris, W. E., & Pritchet, C. J. 2001, AJ, 121, 2557
Ekholm, T., Baryshev, Y., Teerikorpi, P., Hanski, M. O., & Paturel, G. 2001, A&A, 368, L17
Fall, S. M., & Efstathiou, G. 1980, MNRAS, 193, 189

Forman, W., Jones, C., & Tucker, W. 1985, ApJ, 293, 102
Fouqué, P., Solanes, J. M., Sanchis, T., & Balkowski, C. 2001, A&A, 375, 770
Frenk, C. S., & White, S. D. M. 2012, AnP, 524, 507
Giraud, E. 1986, A&A, 170, 1
González, R. E., Kravtsov, A. V., & Gnedin, N. Y. 2013, ApJ, 770, 96
Governato, F., Moore, B., Cen, R., et al. 1997, NewA, 2, 91
Hinshaw, G., Larson, D., Komatsu, E., et al. 2013, ApJS, 208, 19
Hudson, M. J., Gillis, B. R., Coupon, J., et al. 2013, MNRAS, submitted (arXiv:1310.6784)
Humphrey, P. J., Buote, D. A., Canizares, C. R., Fabian, A. C., & Miller, J. M. 2011, ApJ, 729, 53
Joshi, Y. C., Pandey, A. K., Narasimha, D., Sagar, R., & Giraud-Héraud, Y. 2003, A&A, 402, 113
Kahn, F. D., & Woltjer, L. 1959, ApJ, 130, 705
Karachentsev, I. D. 2005, AJ, 129, 178
Karachentsev, I. D. 2012, AstBu, 67, 123
Karachentsev, I. D., Karachentseva, V. E., Huchtmeier, W. K., & Makarov, D. I. 2004, AJ, 127, 2031
Karachentsev, I. D., Kashibadze, O. G., Makarov, D. I., & Tully, R. B. 2009, MNRAS, 393, 1265
Karachentsev, I. D., Makarov, D. I., Sharina, M. E., et al. 2003, A&A, 398, 479
Karachentsev, I. D., Sharina, M. E., Makarov, D. I., et al. 2002, A&A, 389, 812
Klypin, A., Hoffman, Y., Kravtsov, A. V., & Gottlöber, S. 2003, ApJ, 596, 19
Klypin, A., & Holtzman, J. 1997, arXiv:astro-ph/9712217
Klypin, A., & Prada, F. 2009, ApJ, 690, 1488
Klypin, A., Zhao, H., & Somerville, R. S. 2002, ApJ, 573, 597
Klypin, A. A., Trujillo-Gomez, S., & Primack, J. 2011, ApJ, 740, 102
Kravtsov, A., Vikhlinin, A., & Meshscheryakov, A. 2014, ApJ, submitted (arXiv:1401.7329)
Li, Y.-S., & White, S. D. M. 2008, MNRAS, 384, 1459
Macciò, A. V., Governato, F., & Horellou, C. 2005, MNRAS, 359, 941
Mandelbaum, R., Seljak, U., Kauffmann, G., Hirata, C. M., & Brinkmann, J. 2006, MNRAS, 368, 715
Martinez-Vaquero, L. A., Yepes, G., Hoffman, Y., Gottlöber, S., & Sivan, M. 2009, MNRAS, 397, 2070
Mathews, W. G., & Brighenti, F. 2003, ARA&A, 41, 191
McConnachie, A. W., Irwin, M. J., Ferguson, A. M. N., et al. 2005, MNRAS, 356, 979
McKay, T. A., Sheldon, E. S., Johnston, D., et al. 2002, ApJL, 571, L85
Mei, S., Blakeslee, J. P., Côté, P., et al. 2007, ApJ, 655, 144
More, S., van den Bosch, F. C., Cacciato, M., et al. 2011, MNRAS, 410, 210
Moster, B. P., Naab, T., & White, S. D. M. 2013, MNRAS, 428, 3121
Nulsen, P. E. J., & Bohringer, H. 1995, MNRAS, 274, 1093
Prada, F., Vitvitska, M., Klypin, A., et al. 2003, ApJ, 598, 260
Reid, M. J., Menten, K. M., Zheng, X. W., et al. 2009, ApJ, 700, 137
Ribas, I., Jordi, C., Vilardell, F., et al. 2005, ApJL, 635, L37
Roberts, M. S., & Rots, A. H. 1973, A&A, 26, 483
Rubin, V. C., & Ford, W. K., Jr. 1970, ApJ, 159, 379
Sandage, A., & Tammann, G. A. 1975, ApJ, 196, 313
Sohn, S. T., Anderson, J., & van der Marel, R. P. 2012, ApJ, 753, 7
Tikhonov, A. V., & Klypin, A. 2009, MNRAS, 395, 1915
van der Marel, R. P., Fardal, M., Besla, G., et al. 2012, ApJ, 753, 8
van der Marel, R. P., & Guhathakurta, P. 2008, ApJ, 678, 187
van Uitert, E., Hoekstra, H., Velander, M., et al. 2011, A&A, 534, A14
Velander, M., van Uitert, E., Hoekstra, H., et al. 2013, MNRAS, 437, 2111
Watkins, L. L., Evans, N. W., & An, J. H. 2010, MNRAS, 406, 264
White, S. D. M., & Rees, M. J. 1978, MNRAS, 183, 341
Widrow, L. M., & Dubinski, J. 2005, ApJ, 631, 838
Zaritsky, D., Smith, R., Frenk, C., & White, S. D. M. 1993, ApJ, 405, 464
Zaritsky, D., Smith, R., Frenk, C., & White, S. D. M. 1997, ApJ, 478, 39
Zaritsky, D., & White, S. D. M. 1994, ApJ, 435, 599